

Electronic Supplementary Information

Functionalization of metal-organic frameworks with cuprous sites using vapor-induced selective reduction: efficient adsorbents for deep desulfurization

Ju-Xiang Qin, Peng Tan, Yao Jiang, Xiao-Qin Liu*, Qiu-Xia He, and Lin-Bing Sun*

Jiangsu National Synergetic Innovation Center for Advanced Materials (SICAM), State Key Laboratory of Materials-Oriented Chemical Engineering, College of Chemistry and Chemical Engineering, Nanjing Tech University, Nanjing 210009, China.

E-mail: lbsun@njtech.edu.cn

Experimental section

Chemicals

Copper nitrate trihydrate, 1,4-benzenedicarboxylic acid, chromium nitrate monohydrate, terephthalic acid (TPA), hydrofluoric acid (40%), *N,N*-dimethylformamide (DMF), and methanol was obtained from Sinopharm. Thiophene, benzothiophene (BT), 4,6-dimethyldibenzothiophene (DMDBT), and isooctane were purchased from Sigma.

Preparation of MIL-101(Cr)

Briefly, 0.664 g TPA, 1.66 g $\text{Cr}(\text{NO}_3)_3 \cdot 9\text{H}_2\text{O}$, 0.8 mL aqueous HF solution (40%) and 19.2 mL ultrapure water were transformed into a 100 mL Teflon-lined stainless steel autoclave, and then heated up to 220 °C for 8 h. Afterwards, the autoclave was cooled at ambient temperature. The green suspension of MIL-101(Cr) was filtered, washed thoroughly with 150 mL DMF at 150 °C for 12 h to remove the excess TPA, and dried at 100 °C overnight. To remove DMF in the pores, the sample was treated in absolute ethanol at 60 °C for 12 h and dried at 100 °C overnight.

Instrumentation

X-ray diffraction (XRD) patterns of the materials were recorded on a Bruker D8 Advance diffractometer with $\text{Cu K}\alpha$ radiation in the 2θ range from 5° to 60° at 40 kV and 40 mA. The N_2 adsorption-desorption isotherms were measured using an ASAP 2020 apparatus at -196 °C. Prior to analysis, the samples were evacuated at 180 °C for 4 h. The Brunauer-Emmett-Teller (BET) surface area was calculated at relative pressure ranging from 0.05 to 0.25. The total pore volume was derived from the amount adsorbed at a relative pressure of about 0.99. The shapes and morphologies of the materials were observed by field emission scanning electron microscopy (FESEM; HITACHI S-4800). Transmission electron microscopy (TEM) was performed on a JEM-2010UHR electron microscope operated at 200 kV. Fourier transform infrared (FTIR) measurements were performed on a Nicolet Nexus 470 spectrometer by means of the KBr pellet technique. The spectra were collected with a 2 cm^{-1} resolution. UV-Vis spectra were measured with a Cintra 20 (Australian) spectrometer in reflection mode. X-ray photoelectron spectroscopy (XPS) analysis was conducted on a Physical Electronic PHI-550 spectrometer equipped with an Al $\text{K}\alpha$ X-ray source ($h\nu=1486.6$ eV) operating at

10 kV and 35 mA. Quantitative analysis of Cu(I) content in the samples was performed by using a wet chemistry titration method. Cuprous species in the sample was dissolved in 10 mL of a ferric chloride reagent and 50 mL H₂O. The ferric chloride reagent was prepared by dissolving 75 g of ferric chloride in 150 mL of HCl (37%), 400 mL of H₂O, and 5 mL of H₂O₂ (30%), and the reagent was heated till boiling to remove excess H₂O₂. The reaction of Cu(I) with Fe(III) leads to the formation of stable Cu(II) and Fe(II). The amount of Fe(II) was then determined by the titration with ceric sulfate solution (0.0889 mol·L⁻¹), where phenanthroline was employed as an indicator. The mechanism of reaction was processed in a temperature-programmed apparatus equipped with a mass spectrometer (MS). The temperature of the sample was raised linearly at rate of 2 °C min⁻¹ from room temperature up to 600 °C. CH₃OH was introduced into the sample by the means of Ar bubbling.

Adsorption capacity calculation

Breakthrough curves were generated by plotting the normalized sulfur concentration versus the cumulative fuel volume. The normalized concentration (c/c_0) was obtained from the detected content (c) divided by the initial content (c_0), and the cumulative fuel volume was normalized by the adsorbent weight. The adsorption capacity was calculated by integral calculus as shown in Eq. 1.

$$q = \frac{v}{m} \frac{\rho X_0}{M} \int_0^t \left(1 - \frac{c_t}{c_0}\right) dt \quad (1)$$

Where q is the total sulfur adsorbed amount (mmol·g⁻¹), v is the feed volumetric flow rate (mL·min⁻¹), ρ is the fuel density (g·mL⁻¹) at room temperature, X_0 is the total sulfur fraction (by weight) in the feed, c_0 is the total sulfur concentration in the feed (ppmw), m is the weight of the sorbent bed (g), M is the molecular weight of sulfur (g·mol⁻¹), c_t is the effluent total sulfur concentration (ppmw) at time t (min). The integral on the right hand side of Eq. 1 is the area above the breakthrough curves at any time t . The adsorption capacity mentioned in the present study was calculated at saturation; at that time the effluent sulfur concentration was equal to the sulfur concentration in the feed..

Table S1 Structural properties, Cu content, and adsorptive desulfurization performance of different samples

Sample	S_{BET} (m^2/g)	V_{p} (cm^3/g)	Total Cu content ^a (mmol/g)	Cu(I) content ^b (mmol/g)	Cu(I) yield ^c (%)	Uptake of thiophene ($\text{mmol S}/\text{g}$)	
						Breakthrough	Saturation
MIL-101(Cr)	2948	1.57	–	–	–	0.101	0.153
Cu(I)M-1	2051	1.53	1	0.99	99.1	0.143	0.197
Cu(I)M-3	1711	1.15	3	2.99	99.8	0.291	0.373
Cu(I)M-5	1592	1.11	5	4.97	99.4	0.171	0.276

^a Amount of Cu introduced to MIL-101(Cr). ^b Determined by titration. ^c Calculated by $\text{Cu(I)}/[\text{Cu(I)} + \text{Cu(II)}]$.

Table S2 Structure of aromatic sulfur compounds used in the study

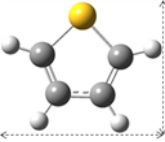

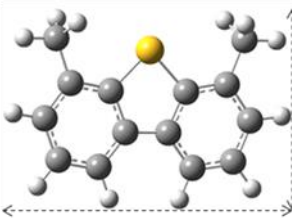
Sulfur compound	Structure	Molecular size (Å)
Thiophene		5.6×7.7
BT		6.5×8.9
DMDBT		7.8×12.3

Table S3 Amount of Cu(I) formed in different MOFs using the VISR strategy

Sample	Total Cu content ^a (mmol/g)	Cu(I) content ^b (mmol/g)	Cu(I) yield ^c (%)
Cu(I)@MIL-101(Cr)	3	2.99	99.8
Cu(I)@MIL-100(Fe)	3	2.98	99.3
Cu(I)@HKUST-1	3	2.97	99.0

^a Amount of Cu introduced. ^b Determined by titration. ^c Calculated by $\text{Cu(I)}/[\text{Cu(I)} + \text{Cu(II)}]$.

Table S4 Amount of Cu(I) formed in MIL-101(Cr) using the VISR strategy with different reducing agents

Reducing agent	Reducing conditions ^a	Total Cu content ^b (mmol/g)	Cu(I) content ^c (mmol/g)	Cu(I) yield ^d (%)
Methanol	200 °C, 6 h	3	2.99	99.8
Ethanol	200 °C, 7 h	3	2.92	97.3
Formaldehyde	160 °C, 10 h	3	1.80	60.0

^a Optimal conditions for the formation of highest yield of Cu(I). ^b Amount of Cu introduced to MIL-101(Cr). ^c Determined by titration. ^d Calculated by $\text{Cu(I)}/[\text{Cu(I)} + \text{Cu(II)}]$.

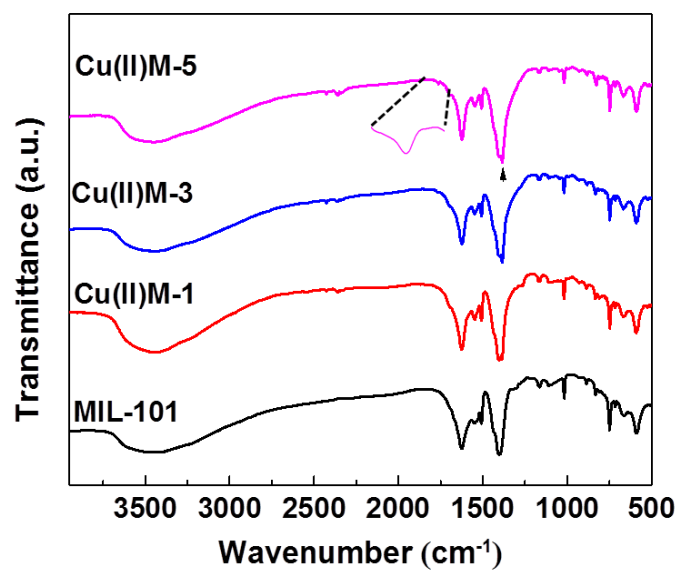


Fig. S1 IR spectra of the samples MIL-101(Cr) and Cu(II)@MIL-101(Cr) with different Cu loading.

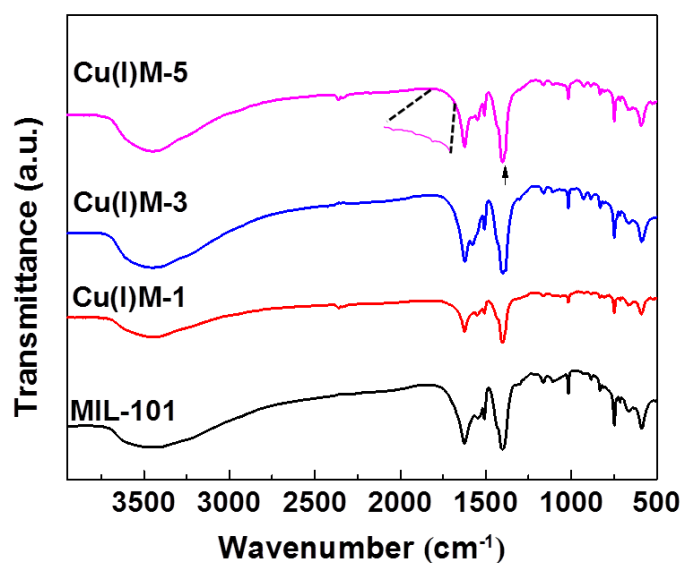


Fig. S2 IR spectra of the samples MIL-101(Cr) and Cu(I)@MIL-101(Cr) with different Cu loading.

IR spectra. The materials before and after VISR treatment were also studied by Fourier transform infrared (IR) spectra. As depicted in Supplementary Figs. 1 and 2, Cu(II)@MIL-101(Cr) exhibit additional bands at 1760 and 1380 cm⁻¹ derived from nitrate in Cu(II) salt as compared to pristine MIL-101(Cr). The intensity of these bands increases with the increase of Cu content. It is interesting to note that the bands at 1760 and 1380 cm⁻¹ disappear after VSIR, indicating that the Cu(II) salt is converted.

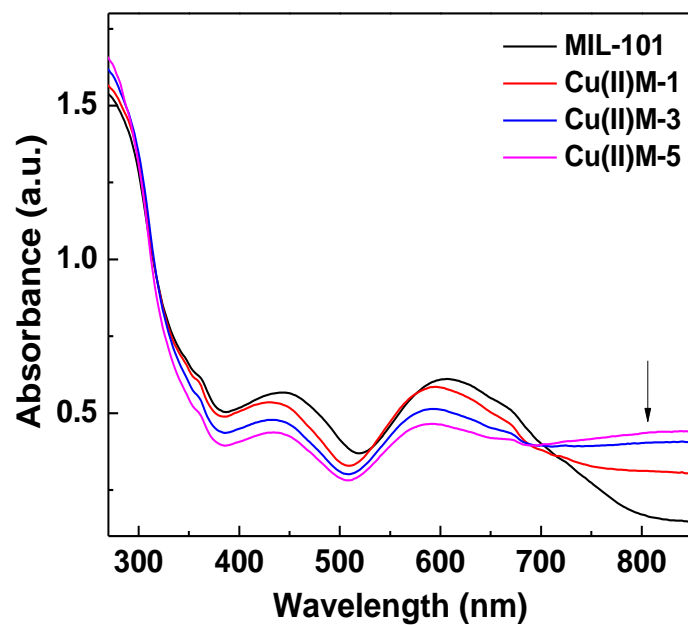


Fig. S3 UV-vis absorption spectra of the samples MIL-101(Cr) and Cu(II)@MIL-101(Cr) with different Cu loading.

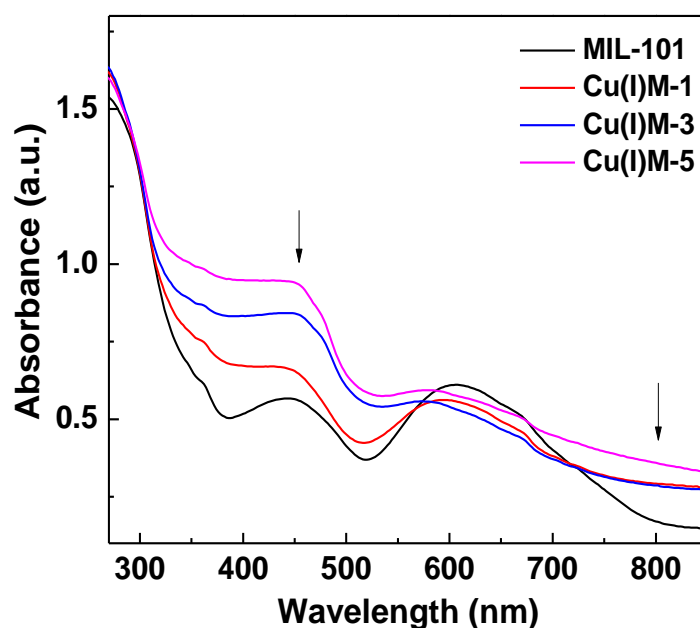


Fig. S4 UV-vis absorption spectra of the samples MIL-101(Cr) and Cu(I)@MIL-101(Cr) with different Cu loading.

UV-vis spectra. UV-vis spectra of the materials before and after VISR treatment were recorded as well. The spectra of pristine MIL-101(Cr) and the materials before and after reduction were shown in Supplementary Figs. 3 and 4. The pristine MIL-101(Cr) displays two broad adsorption peaks at 450 and 607 nm in the visible region, which are attributed to the d-d transition of Cr(III), ${}^4A_{2g} \rightarrow {}^4T_{1g}$ and ${}^4A_{2g} \rightarrow {}^4T_{2g}$, respectively. After introducing Cu(II), the intensity of the two broad adsorption peaks decreases regularly with the increase of Cu content. Also, a certain degree of blue shifting for the two peaks is observable due to the saturation in Cr(III) caused by the increasing electron transition energy. In addition, the intensity of band in the range of 700-800 nm increases for Cu(II)@MIL-101(Cr) materials, which corresponds to the d-d transition of Cu(II). After reduction, the intensity of band for Cu(II) declines; in the meanwhile, a new adsorption band at 450 nm belonged to the d-d transition of Cu₂O emerges. The results from UV-vis spectra give further evidence of the successful conversion of Cu(II) to Cu(I) on MIL-101(Cr).

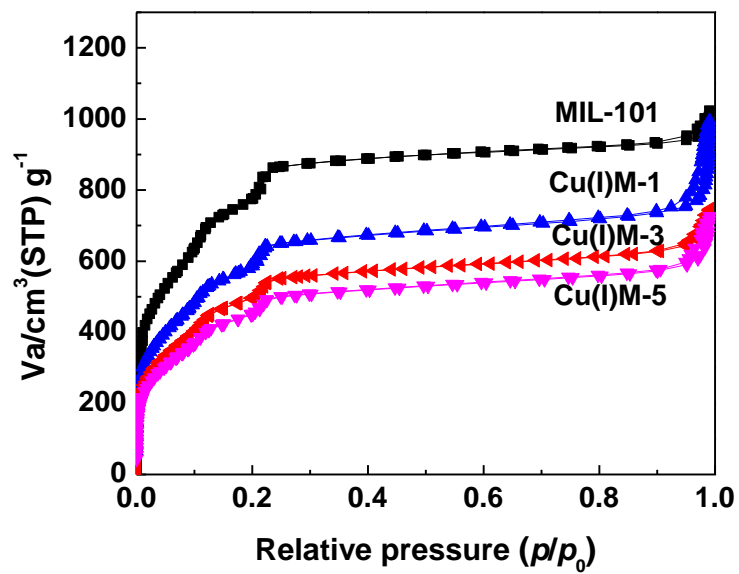


Fig. S5 N₂ adsorption-desorption isotherms of the samples MIL-101(Cr) and Cu(I)@MIL-101(Cr) with different Cu loading.

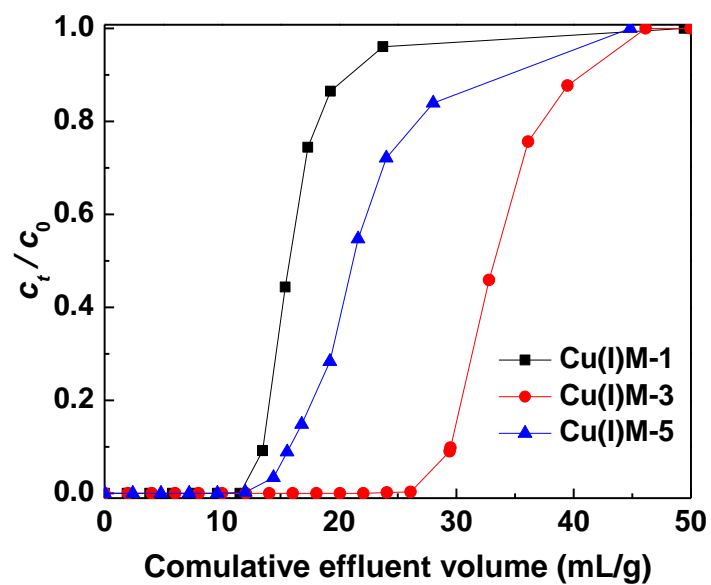


Fig. S6 Breakthrough curves of thiophene in a fixed-bed adsorber with Cu(I)M-1, Cu(I)M-3 and Cu(I)M-5 samples.

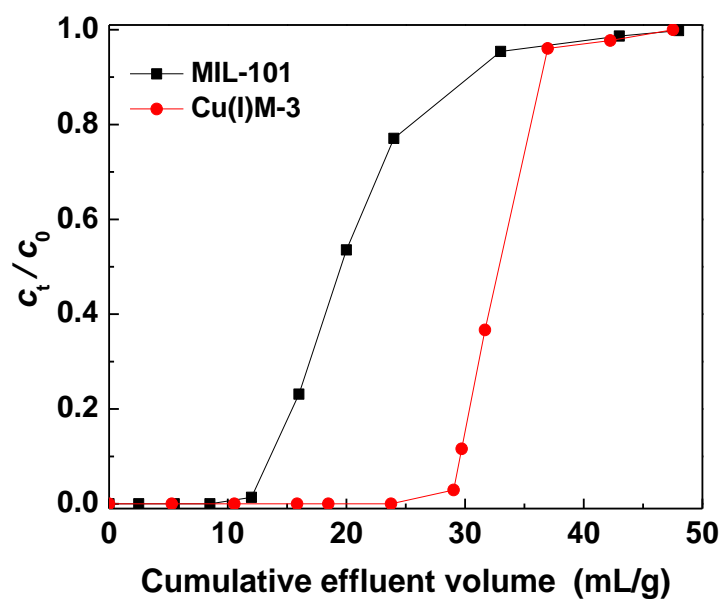


Fig. S7 Breakthrough curves of BT in a fixed-bed adsorber with MIL-101(Cr) and Cu(I)M-3 samples.

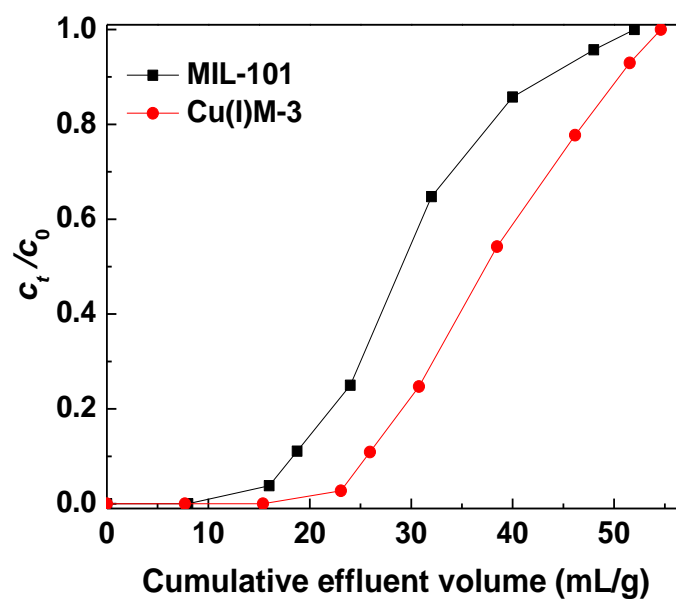


Fig. S8 Breakthrough curves of DMDBT in a fixed-bed adsorber with MIL-101(Cr) and Cu(I)M-3 samples.

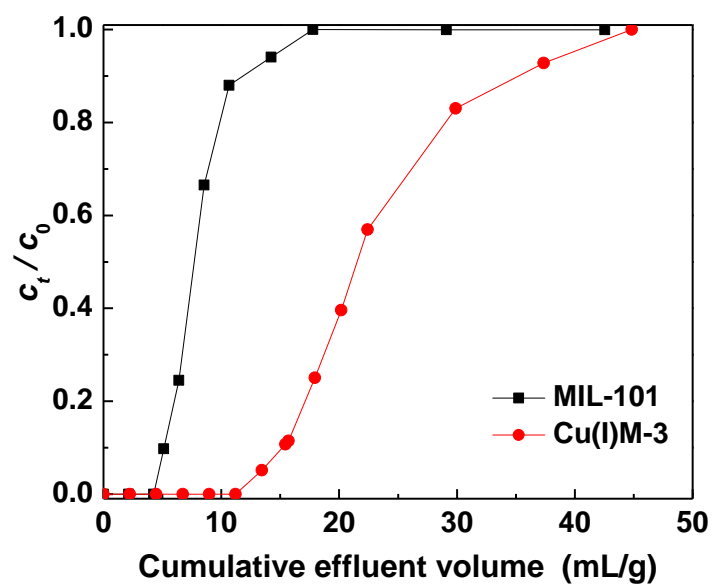


Fig. S9 Breakthrough curves of thiophene in the presence of aromatics in a fixed-bed adsorber with MIL-101(Cr) and Cu(I)M-3 samples.

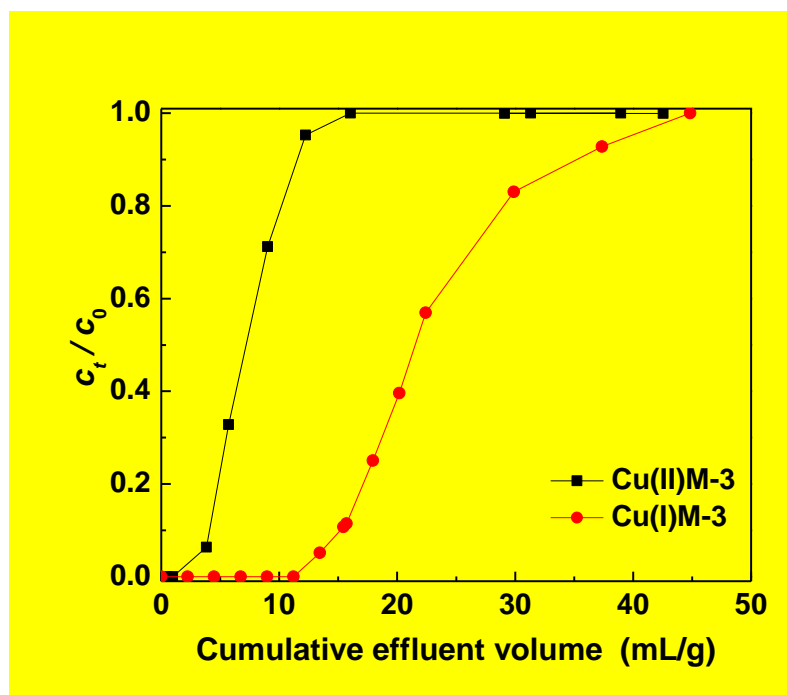


Fig. S10 Breakthrough curves of thiophene in a fixed-bed adsorber with Cu(II)M-3 and Cu(I)M-3 samples.

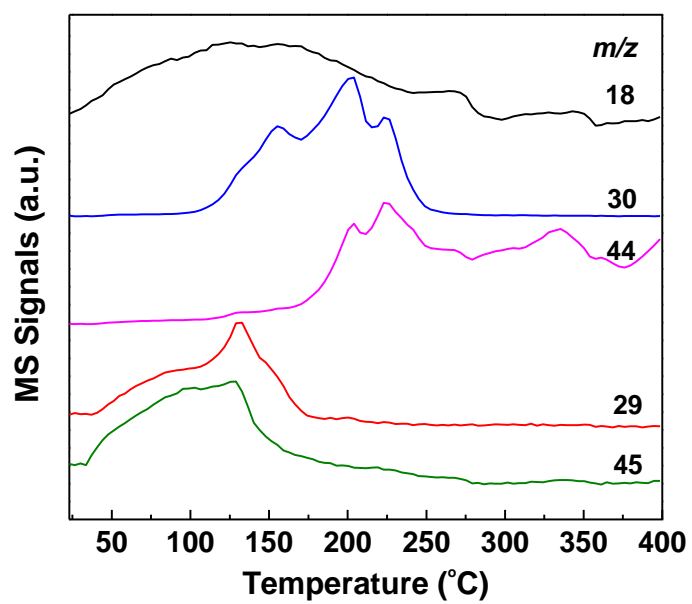


Fig. S11 MS-monitored temperature-programmed reaction of methanol vapor with the sample Cu(II)@MIL-101(Cr).

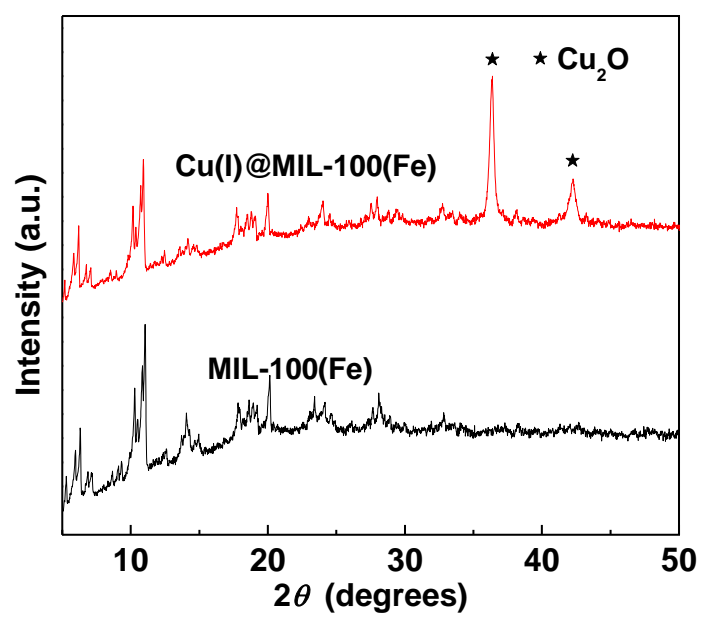


Fig. S12 XRD patterns of the samples MIL-100(Fe) and Cu(I)@MIL-100(Fe).

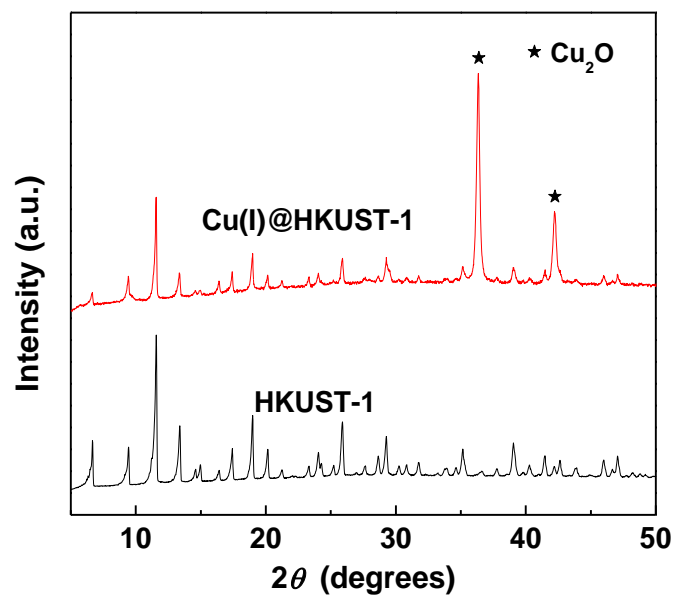


Fig. S13 XRD patterns of the samples HKUST-1 and Cu(I)@ HKUST-1.

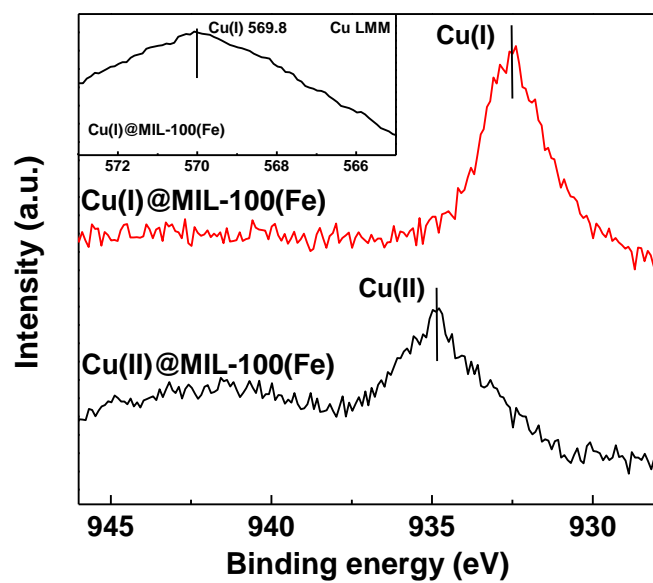


Fig. S14 XPS of Cu(II)@MIL-100(Fe) before and after VISR with methanol vapors.

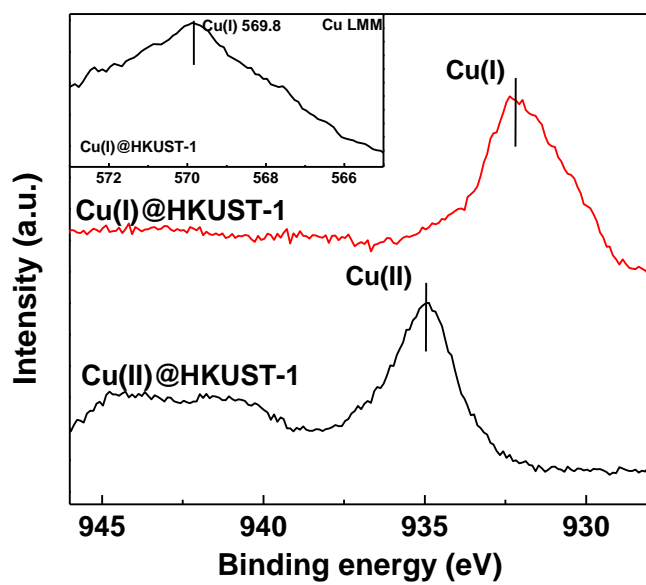


Fig. S15 XPS of Cu(II)@HKUST-1 before and after VISR with methanol vapors.

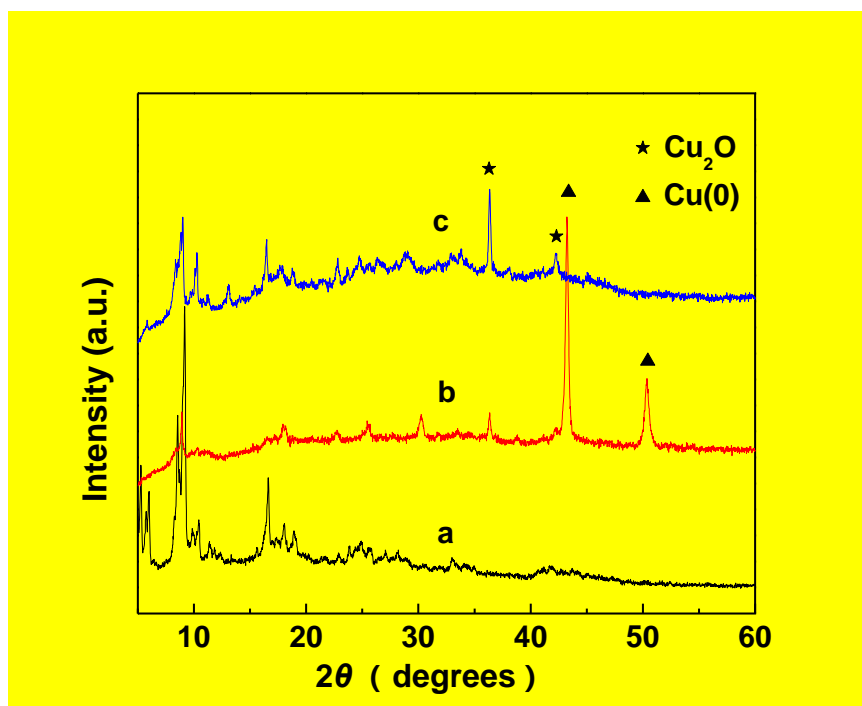


Fig. S16 XRD patterns of the samples (a) MIL-101(Cr) as well as Cu(II)@MCr-3 reduced by (b) paraformaldehyde and (c) the formaldehyde solution.

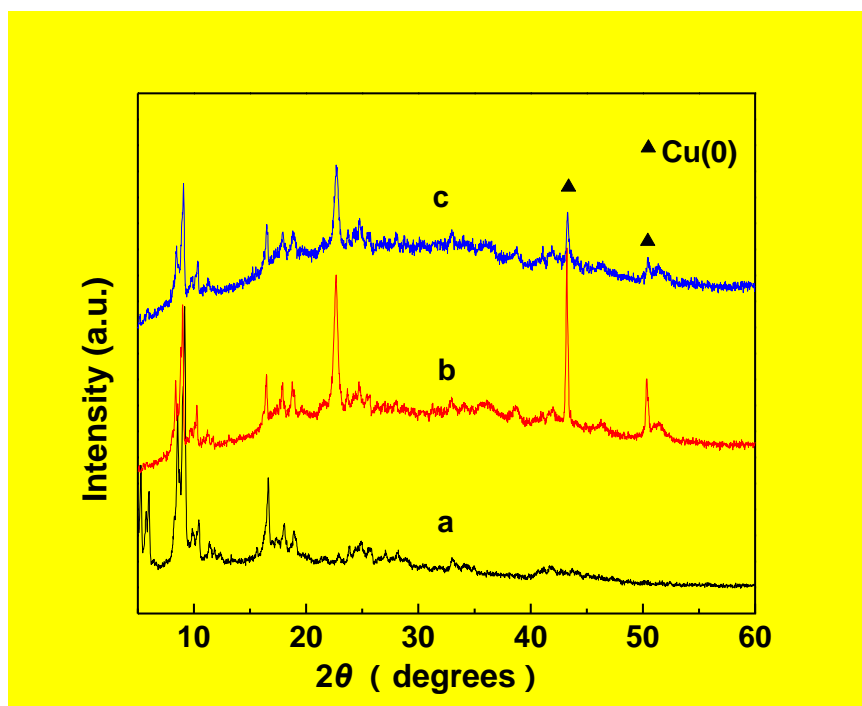


Fig. S17 XRD patterns of the samples (a) MIL-101(Cr) as well as Cu(II)@MCr-3 reduced by glycerol at (b) 160 and (c) 140 °C.

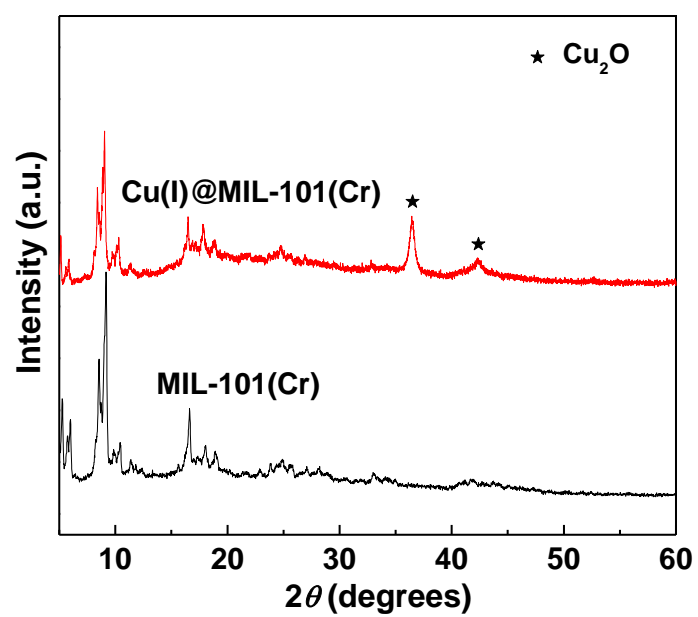


Fig. S18 XRD patterns of the samples MIL-101(Cr) and Cu(I)@MIL-101(Cr) obtained by VISR with ethanol vapors.

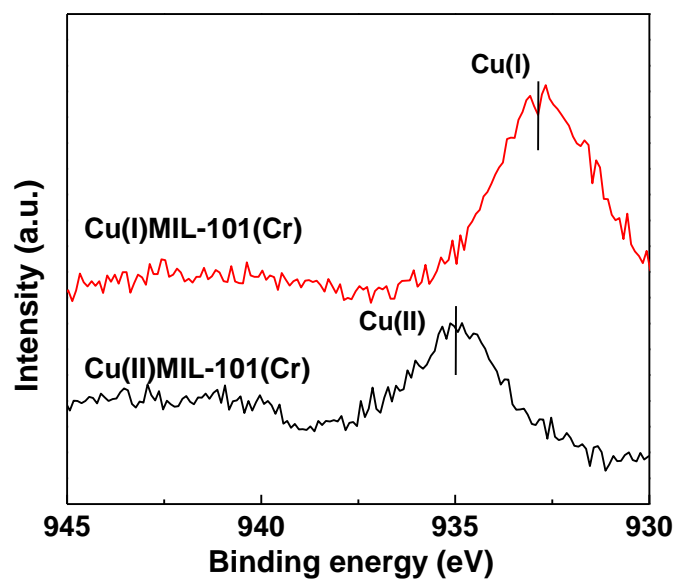


Fig. S19 XPS of the sample Cu(II)@MIL-101(Cr) before and after VISR with ethanol vapors.

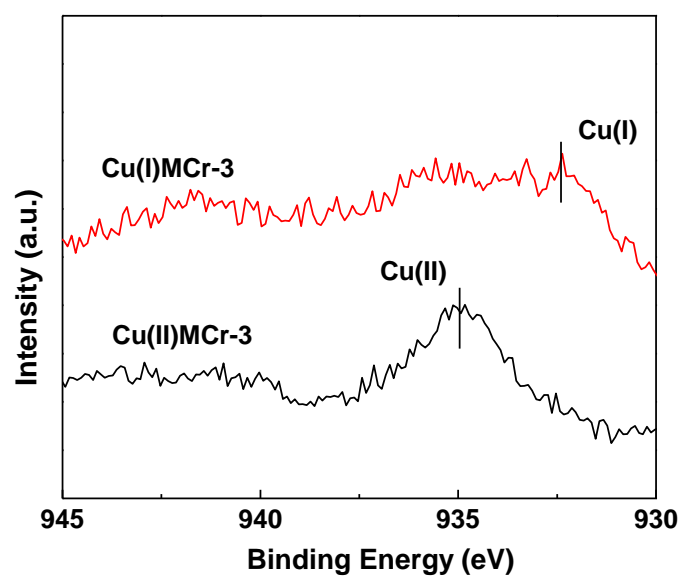


Fig. S20 XPS of the sample Cu(II)@MIL-101(Cr) before and after VISR with formaldehyde vapors.